Channel Modeling and Signal Processing for Array-Based Visible Light Communication System Under Link Misalignment

Jiaqi Wei, Chen Gong, *Senior Member, IEEE*, Nuo Huang, and Zhengyuan Xu, *Senior Member, IEEE*

***Abstract*—We address the lens optimization and signal processing for array-based multiple-input multiple-output (MIMO) visible light communication, especially under link misalignment. We employ one concave lens and one convex lens to separate the lights from different light-emitting diodes (LEDs), and optimize the lens structure to minimize the condition number of channel gain matrix. In this way, the light emitted by different LEDs can be separated well from each other. To further mitigate the interference under transmitter/receiver mobility, we propose two signal processing approaches based on successive interference cancellation (SIC) and multi-layer coding (MC), along with maximum ratio combining (MRC) for interference/signal decoding. It is demonstrated that the interference can be reconstructed and eliminated through SIC, and MC can partially decode the interference to better reconstruct the desirable message. The proposed signal processing approaches can significantly improve the sum rate in both link alignment and misalignment cases. Moreover, MC can achieve higher sum rate, especially in the case of link misalignment.**

***Index Terms*—MIMO, multi-layer coding, optical antenna, signal processing, SIC, visible light communication.**

I. Introduction

With steady development of mobile communication technology, the spectrum resource has become more and more sparse, leading to spectrum crisis. Researchers gradually pay more attention to visible light communication (VLC) that relies on visible light spectrum [1], [2]. At the receiver, the optical signal can be detected by a photodiode (PD) and converted to electrical signal. The data transmission and illumination can be simultaneously realized. VLC provides a feasible alternative to traditional communication and can be adopted as a supplement to the current radio-frequency (RF) communication [3]. The recent advancements of light-emitting diode (LED) technology have also greatly promoted the related research on VLC.

Since the feasibility of VLC was validated [4], there have been steady endeavors. Channel modeling is an important basis. Early research works have been reported in [5]–[8] and the researchers are still working on channel modeling. Reference [9] proposed a modeling method based on ray tracing to characterize the transmission environment more accurately. Existing works have shown good agreement between the simulated and measured channel responses [10], [11]. With multiple LEDs adopted for illumination, multiple input multiple output (MIMO) technology can be applied to increase the data rates [12]–[16]. The diversity of MIMO communication system can compensate the channel loss and improve the system performance [17]. That is, the desirable signals can be detected by multiple receivers, leading to higher performance gain.

In the MIMO VLC system, imaging architecture can be adopted at the receiver to achieve spatial diversity. For such type of system, the design of suitable optical antennas is an essential problem. Hemispherical lens [18], fisheye lens [19] are typically used to provide a wider view while increasing the optical gain, and other different kinds of lenses [20], [21] that can separate light beams and reduce inter-cross are also desirable.

Another issue in MIMO VLC system is the signal interference under link misalignment, which means that the PD receives not only the desired signal, but also the interference signal from adjacent LEDs. Common signal processing methods focus on suppressing interference. Reference [22] conducts an extensive review of representative methods. As for array-based system, it is more suitable to reconstruct and eliminate the interference at the receiver, which adopts successive interference cancellation (SIC). In the classical two-user interference channel, a typical model called rate splitting was proposed by Han-Kobayashi [23], which divides the source into two parts: public and private, and decodes part of the interference if such decoding is helpful. Multi-layer coding (MC) is an extension of Han-Kobayashi (HK) scheme, whose main idea is also interference cancellation. At the transmitter, the data is split into multiple sub-streams which are independent of each other. At the receiver, several layers are divided into groups and decoded simultaneously [24].

In this paper, we establish an indoor VLC system with multiple transmitters and receivers. In order to suppress the interference among light beams, we use a lens group as

Manuscript received January 3, 2022; revised February 11, 2022; accepted March 7, 2022. Date of publication March 15, 2022; date of current version March 24, 2022. This work was supported in part by the National Key Research and Development Program of China under Grant 2018YFB1801904, in part by the National Natural Science Foundation of China under Grants 62171428 and 62101526, in part by the Key Program of National Natural Science Foundation of China under Grant 61631018, in part by the Key Research Program of Frontier Sciences of CAS under Grant QYZDY-SSW-JSC003, and in part by the Fundamental Research Funds for the Central Universities under Grant KY2100000118. *(Corresponding authors: Chen Gong; Nuo Huang.)*

The authors are with the Key Laboratory of Wireless-Optical Communications, Chinese Academy of Sciences, Hefei 230027, China and with the School of Information Science and Technology, University of Science and Technology of China, Hefei 230027, China (e-mail: kellyway@mail.ustc.edu.cn; cgong821@ustc.edu.cn; huangnuo@ustc.edu.cn; xuzy@ustc.edu.cn).

Digital Object Identifier 10.1109/JPHOT.2022.3158893

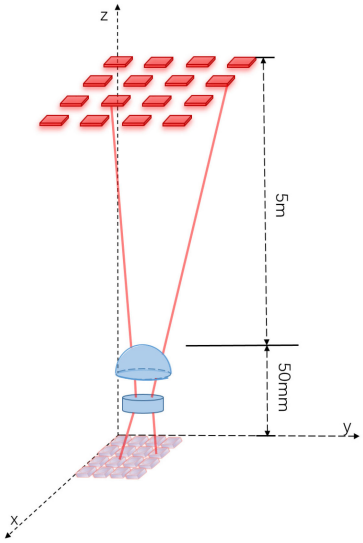

Fig. 1. Configuration of the array-based VLC system under consideration.

optical antenna and optimize the lens group structure. We also investigate the MIMO channel model under link misalignment. Considering the special interference structure of the array-based system, we propose two approaches for signal processing under transmitter/receiver mobility, including SIC and group decoding to eliminate the interference. Significant rate improvement by the proposed approaches is demonstrated over the one treating interference as noise.

The remainder of this paper is organized as follows. Section II describes the array-based VLC system under consideration. Section III presents the optimization of lens structure. Section IV proposes the signal processing approaches for the array-based VLC system. Simulation results and discussions are provided in Section V. Finally, we conclude this work in Section VI.

II. System Model

We consider a typical array-based VLC system including an LED array, a PD array and two lenses for concentrating light. The LED array and PD array consist of $l \times l$ and $p \times p$ elements, respectively; the two lenses include a convex lens and a concave lens, which can narrow the LED beam and project the light from each LED to its corresponding PD component to mitigate the inter-LED interference. Once the transmitter is fixed, the receiver can only move around the center, since the field-of-view angle of the lens is limited. Therefore, we assume that the communication system adopts a low-cost coarse tracking module to guarantee small misalignment under receiver mobility.

An example is shown in Fig. 1, where the LED array and PD array are both composed of 4×4 components. The distance between transmitter plane and receiver plane is set to be 5.05 m, which can meet the requirements of most daily scenes. The key parameters of devices are shown in Table I, where ϕ is the diameter of the lens, element spacing of LEDs/PDs represents the horizontal interval between two elements, and element spacing of lenses represents the vertical distance between two lenses.

TABLE I
Key Parameters of the Array-Based VLC System

	LED	Lens	PD
Size/mm	10×10	$\phi 15$, $\phi 10$	0.6×0.6
Quantity	4×4	2	4×4
Element Spacing/mm	10	20	0.1
Height/cm	505	5, 3	0

Assume that the radiation pattern of the LEDs can be approximated by the Lambertian model, i.e.,

$$I(\phi) \approx I_0(\cos\phi)^{C_n}, \tag{1}$$

where ϕ is the angle of irradiance; I_0 is the center luminous intensity; exponent C_n is greater than or equal to 1, but does not need to be an integer. Larger C_n implies narrower intensity distribution of the light source. For example, when C_n is 10, the half-power angle of LED is approximately 21°. In the considered system, we have $\cos\phi = d_v/d_l$, where d_v represents the vertical distance and d_l represents the Euclidean distance between the transmitter and receiver.

In Section III we will show that the non-line-of-sight (NLOS) or reflection component is significantly weaker than the line-of-sight (LOS) component, such that the LOS component dominates. Therefore, we only take the LOS component into consideration in this work. The array-based communication system can be modeled as a MIMO communication system with $N_t(= l \times l)$ transmitters and $N_r(= p \times p)$ receivers. The received signal $\boldsymbol{y} \in \mathbb{R}^{N_r}$ can be expressed as

$$\boldsymbol{y} = \boldsymbol{H}\boldsymbol{x} + \boldsymbol{n} = \sum_{i=1}^{N_t} \boldsymbol{h}_i x_i + \boldsymbol{n}, \tag{2}$$

where $\boldsymbol{x} \in \mathbb{R}^{N_t}$ is the transmitted signal vector with covariance matrix $\mathbb{E}\{\boldsymbol{x}\boldsymbol{x}^H\} = \boldsymbol{I}$; $\boldsymbol{n} \sim N(0, \sigma_n^2 \boldsymbol{I})$ is the additive white Gaussian noise vector; $\boldsymbol{H} = [h_{ji}] \in \mathbb{R}^{N_r \times N_t}$ is the channel gain matrix with element h_{ji} denoting the channel gain between the i-th LED and j-th PD, and $\boldsymbol{h}_i = [h_{i1}, h_{i2}, h_{i3}, \ldots, h_{iN_r}]^T$ is the i-th column vector of the channel matrix $\boldsymbol{H}$. Moreover, signal x_i is subject to non-negativity, peak and average power constraints for VLC, i.e.,

$$x_i \geq 0, x_i \leq A_i, \mathbb{E}[x_i] \leq \epsilon_i, \forall i = 1, \ldots, N_t, \tag{3}$$

where A_i is the peak optical intensity limit, and ϵ_i is the average optical power limit.

We assume that an AC-coupled APD is adopted to block the DC component. The environmental light will change the DC operation point of the PD receiver, resulting in different signal gains and noise variances in the photoelectric conversion output. In such case, the signal model in the electrical domain and the corresponding signal processing both remain unchanged.

TABLE II
THE OPTIMIZED PARAMETERS OF TWO LENSES

	α_1	α_2	**thickness/mm**
Convex Lens	0.036	0.007	6.875
Concave Lens	-0.08	0.05	2

III. OPTIMIZATION OF LENS STRUCTURE

The two optical lenses (i.e., the convex lens and the concave lens) need to be delicately designed such that the light from each LED can be projected to the corresponding PD with low inter-LED interference. Then, the diagonal elements dominate in the corresponding channel gain matrix. The lens optimization process will be elaborated in this section.

Assume that the two used lenses are both aspheric lenses and the surfaces are paraboloid, which can be expressed as

$$z = \frac{cr^2}{1+\sqrt{1-(1+k)c^2r^2}} + \alpha r^2 + \beta r^4 + \cdots, \quad (4)$$

where z is the sag of the lens surface; c represents the radius of curvature; r represents the distance from the lens edge to central axis; k denotes the conic constant; α and β denote the coefficients of quadratic and quartic term. For simplicity, we only consider the quadratic term in (4) and set c and β of each lens to be zero [25]. As a result, (4) can be simplified as $z = \alpha r^2$.

We adopt Zemax, a comprehensive optical design and simulation software, for the lens optimization. Given parameters such as geometric position and refractive index of the object, the direction and intensity of light can be determined. We simulate the array-based VLC system model using Zemax software based on the tracing of light paths. Then, we can readily obtain the channel gain matrix through MATLAB-based extension program.

Condition number is the ratio between the largest and smallest singular values of a matrix, and the condition number of channel gain matrix measures the sensitivity of communication system. Therefore, we optimize the structure of the two lens to minimize the condition number (denoted by κ) of the channel gain matrix corresponding to the received light spots. Specifically, the optimized structure parameters are chosen to be the quadratic coefficients of the front and back surfaces, denoted by $\alpha_1^1, \alpha_2^1, \alpha_1^2, \alpha_2^2$, where superscript 1 (2) represents the convex (concave) lens, and subscript 1 (2) represents the front (back) surface.

Remark 1: The PD receives the desired signal with the strongest power when each light spot falls on one and only one PD (e.g., Fig. 1). Therefore, in optimizing the lens structure, we only consider the case of link alignment, where the channel gain matrix can be approximated as a diagonal matrix. For optimizing the lens structure under link misalignment, additional constraints and different objective need to be considered, such as signal intensity, which remains for future work.

Through exhaustive search method, we can obtain the optimal structure parameters of the two lenses, as given in Table II. The corresponding condition number is 1.6622, and the spot pattern on receiver plane is shown in Fig. 2.

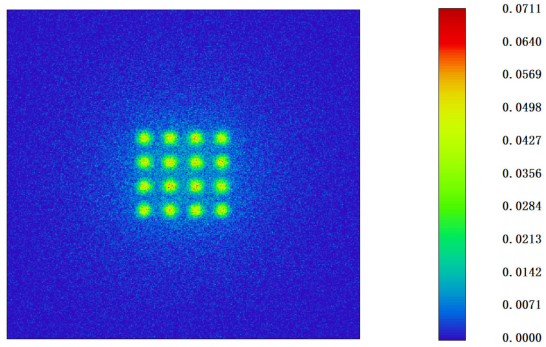

Fig. 2. Spot pattern on the detector plane using a 10 mm× 10 mm detector.

From Fig. 2, it can be seen that the adjacent light spots are easy to distinguish, which implies that the light beams can be well separated and the interference can be suppressed. Moreover, the size of each spot is about 0.5 mm×0.5 mm, which is around $1/20$ of LED size (10 mm×10 mm), demonstrating the good concentrating ability of the optical lenses. The corresponding channel gain matrix is presented in Fig. 3, where the diagonal elements are significantly larger than the off-diagonal ones.

To evaluate the influence of NLOS (or reflection) component, we consider an empty room of size 5 m × 5 m × 5.05 m, and assume that the materials of six surfaces follow purely diffuse reflection model. The VLC system is located in the center of the room, as shown in Fig. 4. After simulating the environment in ZEMAX, we obtain the spot pattern on the detector plane as shown in Fig. 5. We can see that even in the scenario with both LOS and NLOS components, the shapes of the received light spots are similar with clear outline. The interference at the PD array center is relatively strong, but the same subsequent signal processing approach can be applied.

Consider the more general scenario where the transmitter and receiver are not perfectly aligned. In this case, the spatial distribution of light from the LEDs deviates from the position of the PD array, resulting in one light spot covering multiple adjacent PDs and one PD covered by the spots from multiple adjacent LEDs, as shown in Fig. 6. There are sixteen rectangular detectors in this figure, and the colored rectangles represent the LED spots on detector plane. Clearly, as the receiver moves, the light spots may cover two or four detectors.

In this work, we get the most suitable spot size by optimizing the lens, where the condition number of the channel is minimized. In practice, we do not expect the spot size to be larger than the PD size, which wastes light power and possibly causes interference. For the case where the light spot is smaller than the PD size, the interference structure of the array-based system is not affected. Besides, it is also reasonable to assume circular LEDs, where the interference structure is similar and the same approach can be applied accordingly.

Noting that each receiver may be covered by the light spots from multiple LEDs, the communication can be modeled by an interference channel. Due to the specific structure of the interference channel, the transmitted information can be extracted

$$\boldsymbol{H} = \begin{pmatrix}
445.88 & 27.71 & 11.90 & 6.40 & 27.69 & 17.94 & 9.75 & 6.28 & 11.10 & 9.75 & 7.57 & 5.37 & 6.37 & 5.93 & 5.01 & 3.91 \\
31.94 & 450.20 & 29.00 & 11.61 & 18.14 & 28.00 & 17.75 & 10.06 & 10.18 & 11.40 & 9.67 & 7.35 & 5.98 & 6.70 & 6.20 & 5.54 \\
12.05 & 29.67 & 451.72 & 29.95 & 9.80 & 17.46 & 28.14 & 18.46 & 7.56 & 10.24 & 10.99 & 9.71 & 4.75 & 6.37 & 6.55 & 6.07 \\
5.95 & 11.07 & 27.88 & 443.46 & 6.47 & 9.53 & 17.06 & 27.42 & 5.21 & 7.09 & 9.23 & 11.39 & 3.79 & 5.38 & 5.94 & 6.81 \\
31.40 & 18.29 & 9.97 & 6.32 & 450.96 & 27.82 & 10.62 & 6.54 & 29.00 & 17.49 & 10.35 & 6.28 & 11.61 & 9.41 & 7.07 & 4.91 \\
19.04 & 32.04 & 18.73 & 9.95 & 31.03 & 452.33 & 29.08 & 11.18 & 18.54 & 29.31 & 18.15 & 10.18 & 9.64 & 11.05 & 9.81 & 7.04 \\
9.56 & 19.28 & 31.43 & 19.45 & 11.98 & 29.42 & 452.16 & 31.05 & 10.28 & 18.43 & 28.87 & 18.69 & 7.09 & 10.14 & 11.35 & 9.73 \\
5.88 & 10.16 & 18.47 & 29.93 & 6.55 & 10.96 & 27.64 & 446.16 & 6.32 & 9.39 & 17.47 & 29.61 & 5.42 & 7.49 & 9.21 & 11.18 \\
11.37 & 9.75 & 6.90 & 4.76 & 28.46 & 18.11 & 9.66 & 6.04 & 453.32 & 28.12 & 11.88 & 6.35 & 30.28 & 18.59 & 9.76 & 5.85 \\
10.39 & 11.99 & 10.33 & 6.97 & 18.61 & 29.72 & 18.08 & 9.87 & 30.34 & 457.93 & 29.33 & 11.70 & 18.94 & 32.27 & 18.73 & 9.66 \\
7.14 & 9.81 & 11.29 & 9.83 & 9.63 & 18.36 & 29.46 & 18.71 & 11.31 & 30.12 & 456.41 & 31.12 & 9.62 & 18.77 & 31.58 & 19.15 \\
5.20 & 7.07 & 9.66 & 11.89 & 6.03 & 9.50 & 17.86 & 29.22 & 6.56 & 11.62 & 27.06 & 450.99 & 6.00 & 9.65 & 17.78 & 32.14 \\
6.68 & 6.03 & 5.12 & 4.22 & 11.45 & 10.15 & 7.41 & 4.96 & 28.72 & 17.53 & 9.39 & 6.25 & 447.29 & 27.78 & 10.68 & 6.96 \\
5.77 & 6.24 & 5.77 & 5.39 & 9.73 & 11.63 & 9.86 & 6.75 & 18.46 & 27.19 & 17.89 & 9.88 & 31.15 & 455.03 & 28.76 & 11.40 \\
5.09 & 6.12 & 6.70 & 5.92 & 6.74 & 9.56 & 11.35 & 9.73 & 9.79 & 17.27 & 27.15 & 17.51 & 10.93 & 28.74 & 447.49 & 30.92 \\
4.10 & 5.45 & 5.95 & 6.40 & 5.35 & 6.73 & 9.47 & 10.99 & 6.13 & 9.61 & 17.48 & 27.50 & 6.64 & 11.27 & 28.23 & 444.46
\end{pmatrix} \times 10^{-7}$$

Fig. 3. Channel gain matrix of the aligned system.

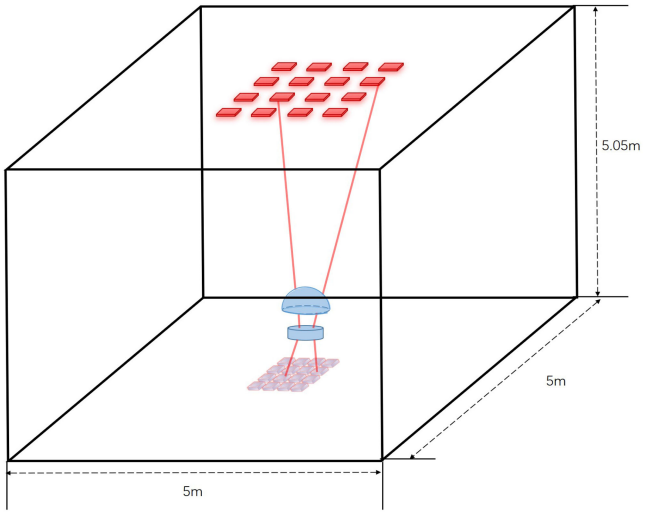

Fig. 4. Illustration of the array-based VLC system in a 5 m × 5 m × 5.05 m room.

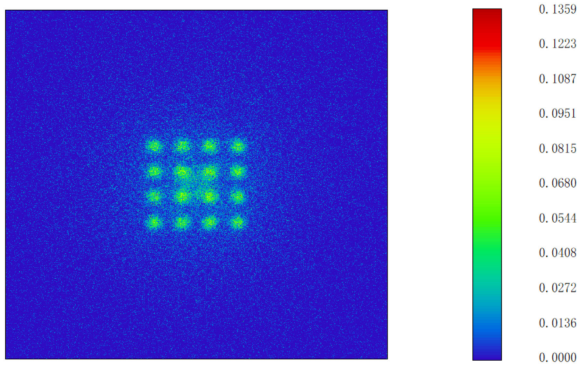

Fig. 5. Spot pattern under LOS+NLOS link with VLC system at the center of the room.

through SIC. The SIC process will be elaborated in the following sections.

For mobile communication, we prefer system with large moving range. However, the moving ranges of VLC transmitter and receiver are limited due to small PD size. Note that more PDs can increase the signal reception area and thus allow larger moving ranges of LEDs and PDs. In the following, we adopt an 8×8 PD array while keeping the same PD size and interval as those in Table I.

Remark 2: For multi-colored VLC system with filters, the interference structure is different due to weak inter-color interference, if the optical filter is adopted at the receiver to remove the out-of-band interference. The spot pattern on the detector plane under link alignment is shown in Fig. 7(a), where each PD is equipped with only one single-color ideal filter with zero transmittance for wavelengths outside the bandpass range. When LEDs/PDs move slightly, the spot pattern is shown in Fig. 7(b). In such case, the inter-signal interference is much weaker than that in a single-color system, but the signal processing approaches in Section IV are still applicable. If the optical spots move away from the corresponding optical filter, the receiver will hardly receive desired signals due to the presence of optical filters.

IV. Signal Processing for Array-Based VLC System

In this section, we first characterize the interference channel of the proposed array-based VLC system in the case of link misalignment. Then, we specify two signal processing methods for such type of channel.

A. Interference Cancellation and Signal Combining

From Fig. 6, the channel of misaligned system can be seen as a superposition of multiple Z-channels. Such channel structure allows SIC for interference processing with low complexity [26].

The idea of SIC is removing the interference signal from the received signal, one at a time as each signal is detected [27]. For example, the transmitter shifts towards the bottom-right in Fig. 6. The detector in the upper-left corner receives the signal without interference from adjacent LEDs, so the decoding starts from the upper-left corner receiver. After this signal is detected, the recovered information is used to subtract the corresponding interference from the received signal. Subsequently, the detector in row 1, column 2 (or the detector in row 2, column 1) contains no interference from adjacent LEDs. Its received signal is detected and the corresponding interference is canceled. Through

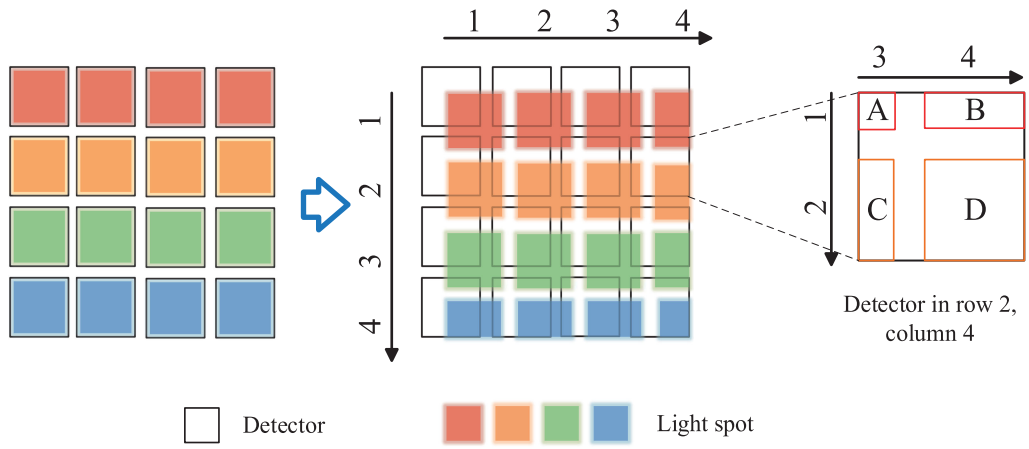

Fig. 6. Spot pattern of mobile system.

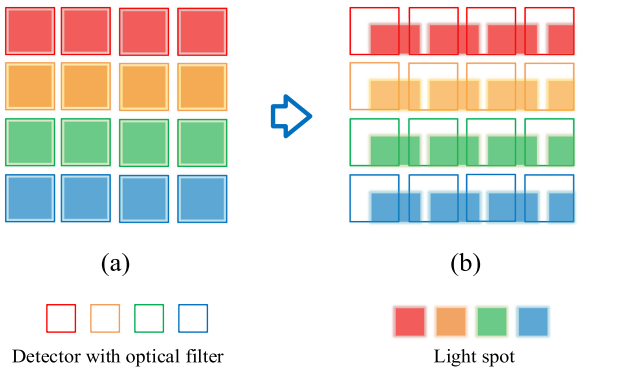

Fig. 7. Spot pattern of multi-color system in different situations. (a) Link alignment. (b) Link misalignment.

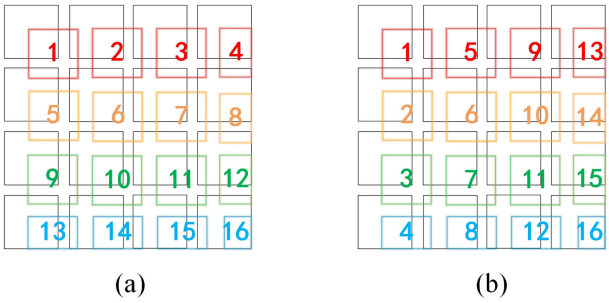

Fig. 8. Decoding order of the proposed system.

similar decoding/cancellation process, all the transmitted data can be recovered in proper order.

Specifically, we assume that the PDs can receive the signals from multiple LEDs. Take the detector in row 2, column 4 for example, as shown in the right-hand side of Fig. 6. This detector receives four different signals, denoted as A, B, C and D. After eliminating the interferences from A, B, C, the signal D can be decoded. According to the above idea of SIC, the 16 signals can be decoded in the order shown in Fig. 8(a) or Fig. 8(b).

Note that the light from one LED may fall on multiple detectors simultaneously. In order to decode the data from each LED, we perform maximum ratio combining (MRC) on the signals received by the corresponding PDs. We set different weights for the received signals of different PDs, and the weight vector corresponding to the j-th transmitted data can be expressed as

$$\boldsymbol{w}_j = \left(w_{j1}, w_{j2}, \ldots, w_{jN_r}\right)^T. \tag{5}$$

For simplicity, the transmitters are labeled according to the decoding order at the receiver side. In decoding the j-th transmitted signal after canceling the interferences from the 1st to the $(j-1)$-th signal, the signal after combining can be expressed as

$$y_j^{co} = \boldsymbol{w}_j^T \boldsymbol{y}_{-(j-1)} = \boldsymbol{w}_j^T \boldsymbol{h}_j x_j + \boldsymbol{w}_j^T \sum_{i=j+1}^{N_t} \boldsymbol{h}_i x_i + \boldsymbol{w}_j^T \boldsymbol{n}, \tag{6}$$

where $\boldsymbol{y}_{-(j-1)} = \sum_{i=j}^{N_t} \boldsymbol{h}_i x_i + \boldsymbol{n}$ denotes the obtained signal vector after subtracting the 1st to the $(j-1)$-th interference signal from the received signal $\boldsymbol{y}$ in (2).

Assuming the interferences from the 1st to the $(j-1)$-th signal are totally canceled, the signal-to-interference-plus-noise ratio (SINR) for decoding x_j from y_j^{co} is

$$SINR_j = \frac{P_{S_j}}{P_{I_j} + P_{N_j}} = \frac{(\boldsymbol{w}_j^T \boldsymbol{h}_j)^2}{\sum_{i=j+1}^{N_t} (\boldsymbol{w}_j^T \boldsymbol{h}_i)^2 + ||\boldsymbol{w}_j||^2 \sigma_n^2}, \tag{7}$$

where P_{S_j} is signal power, P_{I_j} is total interference power, and P_{N_j} is noise power. The optimal weight vector maximizing $SINR_j$ is given by

$$\boldsymbol{w}_j^T = \boldsymbol{h}_j^T \left(\sum_{i=j+1}^{N_t} \boldsymbol{h}_i \boldsymbol{h}_i^T + \sigma_n^2 \boldsymbol{I} \right)^{-1}. \tag{8}$$

In this work, we approximate the VLC channel capacity by using a truncated Gaussian (TG) input distribution with mean $\hat{\mu}$ and variance $\hat{v}^2$ which is given by

$$\theta_{\mu,v}^A(x) = \begin{cases} \rho g_{\mu,v}(x), & x \in [0, A]; \\ 0, & \text{otherwise}; \end{cases} \tag{9}$$

where $g_{\mu,\upsilon}(x)$ is the original Gaussian distribution with mean μ and variance υ^2; $\rho = (G_{\mu,\upsilon}(A) - (G_{\mu,\upsilon}(0))^{-1}$ with $G_{\mu,\upsilon}(x)$ being the corresponding cumulative Gaussian distribution function. Based on the signal constraints in (3), the mean and variance for signal j can be determined as

$$\begin{aligned}\hat{\mu}_j &= \upsilon_j^2[\theta^{A_j}_{\mu_j,\upsilon_j}(0) - \theta^{A_j}_{\mu_j,\upsilon_j}(A_j)] + \mu_j,\\ \hat{\upsilon}_j^2 &= \upsilon_j^2[1 - A_j\theta^{A}_{\mu_j,\upsilon_j}(A_j) - \hat{\mu_j}(\theta^{A_j}_{\mu_j,\upsilon_j}(0) - \theta^{A_j}_{\mu_j,\upsilon_j}(A_j))],\end{aligned} \tag{10}$$

where μ_j and υ_j^2 are the mean and covariance of the original Gaussian distribution for signal j. The achievable rate can be derived as [28]

$$\begin{aligned}R_j = &-\frac{1}{2}\log\left(\upsilon_j^2 - \frac{\underline{h}_{jj}^2\hat{\upsilon}_j^4}{\underline{h}_{jj}^2\hat{\upsilon}_j^2 + \sum_{i=j+1}^{N_t}\underline{h}_{ji}^2\hat{\upsilon}_i^2 + ||\boldsymbol{w}_j||^2\sigma_n^2}\right)\\ &+\frac{1}{2}\log\upsilon_j^2 - \phi_j,\end{aligned} \tag{11}$$

where $\phi_j = \log(\rho_j) + \frac{1}{2}((A_j - \mu_j)\theta^{A_j}_{\mu_j,\nu_j}(A_j) + \mu_j\theta^{A_j}_{\mu_j,\upsilon_j}(0))$ and $\underline{h}_{ji} = \boldsymbol{w}_j^T\boldsymbol{h}_i$.

B. Multi-Layer Coding and Group Decoding

According to Han-Kobayashi [23], the interference channel can be modeled as each transmitter sending both "private" and "common" information. Multi-layer coding and group decoding extend the idea of HK model, via splitting the message into more layers and ensuring higher decoding freedom. To further improve the system performance, we perform multi-layer coding in this work.

At each transmitter, the message is divided into multiple parts and treated as separate layers. Let L_i denote the number of layers at transmitter i, and (i,k) denote layer k at transmitter i. The message sent by one real user can be viewed as the superposition of messages from L_i virtual users, i.e.,

$$x_i = \sum_{k=1}^{L_i} x_{ik}. \tag{12}$$

Assuming equal power allocation for all layers at each transmitter, the power allocated to each layer of transmitter i is $\mathbb{E}[x_i^2]/L_i = 1/L_i$. The constraints on signal x_{ik} are

$$x_{ik} \geq 0, x_{ik} \leq A_{ik}, \mathbb{E}[x_{ik}] \leq \epsilon_{ik}, \forall i = 1,\ldots,N_t, \tag{13}$$

where $A_{ik} = A_i/L_i$ is the peak optical intensity limit, and ϵ_{ik} is the average optical power limit.

The rate of transmitter i is the sum of all virtual users, i.e.,

$$R_i = \sum_{k=1}^{L_i} R_{ik}, \tag{14}$$

where R_{ik} is the rate of layer (i,k). With multi-layer coding at the transmitter, the received signal in (2) can be further rewritten as

$$\underline{\boldsymbol{y}} = \sum_{i=1}^{N_t}\boldsymbol{h}_i x_i + \boldsymbol{n} = \sum_{i=1}^{N_t}\sum_{k=1}^{L_i}\boldsymbol{h}_i x_{ik} + \boldsymbol{n}. \tag{15}$$

Multi-layer coding can increase the flexibility of decoding interference, yielding better transmission performance. To further increase the detection reliability, the receiver can adopt group decoding method, where partial interference is decoded along with the desirable signal. The layers that have not been decoded are treated as noise together with Gaussian noise. For simplicity, we assume that only one layer is decoded at one time. We define the set $\mathcal{G} = \{(i,k)|x_{ik}$ has not been decoded$\}$.

Assume that layer $(i,'k')$ is decoded in the j-th decoding stage. Similarly as in Section IV-A, we combine signals received by multiple PDs at a time, and the weight vector is given by

$$\underline{\boldsymbol{w}}_j = \left(\underline{w}_{j1}, \underline{w}_{j2}, \ldots, \underline{w}_{jN_r}\right)^T. \tag{16}$$

With multi-layer coding, the signal after the j-th combining at the receiver is expressed as

$$\underline{y}_j^{co} = \underline{\boldsymbol{w}}_j^T\boldsymbol{h}_{i'}x_{i'k'} + \underline{\boldsymbol{w}}_j^T\sum_{(i,k)\in\mathcal{G}}\boldsymbol{h}_i x_{ik} + \underline{\boldsymbol{w}}_j^T\boldsymbol{n}. \tag{17}$$

Define $\tilde{\boldsymbol{h}}_i = \sqrt{\frac{1}{L_i}}\boldsymbol{h}_i$. The weight vector can be derived in a similar way as (7) and (8):

$$\underline{\boldsymbol{w}}_j^T = \tilde{\boldsymbol{h}}_{i'}^T\left(\sum_{i=1}^{N_t}G_i\tilde{\boldsymbol{h}}_i\tilde{\boldsymbol{h}}_i^T + \sigma_n^2\boldsymbol{I}\right)^{-1}, \tag{18}$$

where G_i denotes the number of layers belonging to $\mathcal{G}$ for transmitter i.

For each layer, we adopt independent TG distribution and the achievable rate in the j-th decoding stagecan be derived as

$$\begin{aligned}R_j = &-\frac{1}{2}\log\big(\upsilon_{i'k'}^2\\ &-\frac{\underline{h}_{ji'}^2\hat{\upsilon}_{i'k'}^4}{\underline{h}_{ji'}^2\hat{\upsilon}_{i'k'}^2 + \sum_{l=1}^{g}\underline{h}_{j\mathcal{G}[l]}^2\hat{\upsilon}_{\mathcal{G}[l]}^2 + ||\boldsymbol{w}_j||^2\sigma_n^2}\Big)\\ &+\frac{1}{2}\log\upsilon_{i'k'}^2 - \phi_{i'k'},\end{aligned} \tag{19}$$

where $\phi_{ik} = \log\rho_{ik} + \frac{1}{2}[(A_{ik} - \mu_{ik})\theta^{A_{ik}}_{\mu_{ik},\nu_{ik}}(A_{ik}) + \mu_{ik}\theta^{A_{ik}}_{\mu_{ik},\upsilon_{ik}}(0)]$, μ_{ik} and $\hat{\upsilon}_{ik}^2$ are the parameters of the TG distribution for layer (i,k) as in (9), and $g = |\mathcal{G}|$.

One crucial issue of group decoding is to determine the decoding order. Taking the overall performance into account, we aim to maximize the minimum rate among all the layers. The corresponding optimization problem is formulated as

$$\hat{\boldsymbol{q}} = \arg\max_{\boldsymbol{q}\in\mathcal{Q}}\min_{1\leq i\leq L}R_i(\boldsymbol{q}), \tag{20}$$

where $\boldsymbol{q} = [q_1, q_2, q_3, \ldots, q_L]$ denotes the decoding order, $L = \sum_{i=1}^{N_t}L_i$ denotes the total number of layers, $\mathcal{Q}$ is the set of all legitimate decoding orders, and $R_i(\boldsymbol{q})$ represents the achievable rate for the i-th layer in decoding order $\boldsymbol{q}$.

Problem (20) can be solved simply using exhaustive search or dynamic programming. Besides, it can be improved by distributed algorithm. We can define a rate increment margin. If the rate of decoded layers increases beyond the margin after decoding (i,k), then decoding (i,k) may cause an outage.

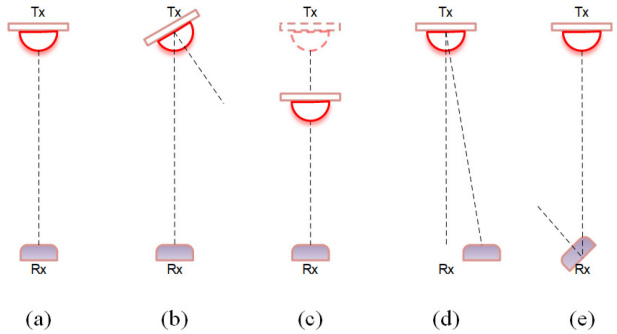

Fig. 9. Relative positions of transmitter and receiver in different cases. (a) Aligned link. (b) Rotated transmitter. (c) Vertically shifted transmitter. (d) Horizontally shifted transmitter. (e) Rotated receiver.

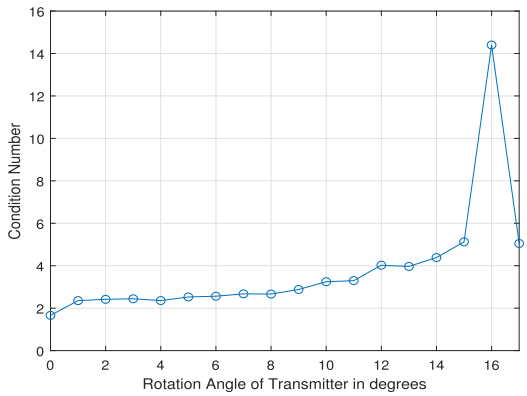

Fig. 10. The condition number of $\boldsymbol{H}$ versus rotation angle of the transmitter.

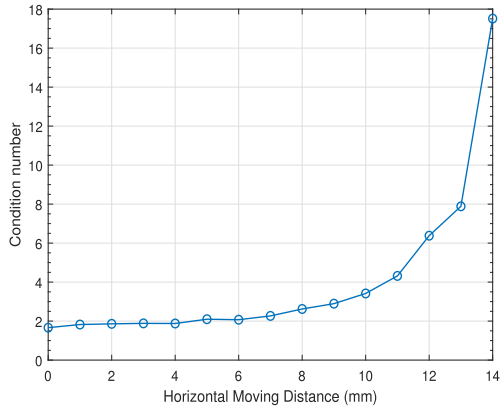

Fig. 11. The condition number of $\boldsymbol{H}$ versus receiver Δ_h.

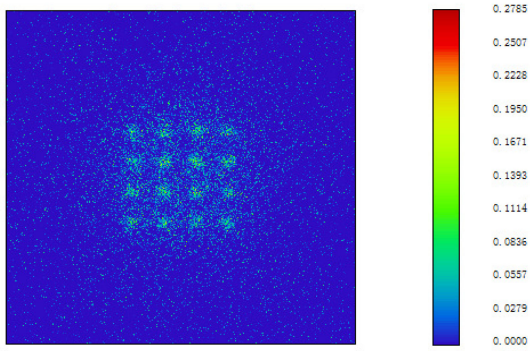

Fig. 12. The spot pattern on detector plane when $\Delta_v = 370$.

The rate increment should be dynamically updated after each decoding. Detailed steps of such algorithm can be found in [29].

Remark 3: Beyond link misalignment, excessive environmental background light will cause APD saturation, which degrades the performance of SIC and MC. Placing optical attenuation slice in front of the receiver PD array can effectively solve such problem [30]. Besides, nonideal lens will cause imaging distortion and aggravate the interference, which can be compensated by digital signal processing.

V. Result Analysis

This section presents the analysis on link misalignment and the simulation results regarding signal processing. We first discuss possible moving direction and range of the optimized 16×16 MIMO system. Then, we increase the number of PDs to 64 for communication and compare the achievable rates under different motion states.

A. Moving Range of Transmitter and Receiver

In practical applications, the VLC transmitter and receiver may be inclined or in offset, resulting in link misalignment as shown in Fig. 9. Therefore, we first explore how channel characteristics change under link misalignment.

In order to measure the relative moving distance over the PD array size, we define Δ_h (Δ_v) as the ratio of moving distance over PD array side length in the horizontal (vertical) direction. In the proposed array-based system, the 4×4 PD array size is 2.7 mm$\times$2.7 mm and the 8×8 PD array size is 5.5 mm$\times$5.5 mm.

Here we assume that the relative position between LED (PD) components is fixed. We adopt the case of link alignment as a baseline. Fig. 10 presents the condition number κ of the channel gain matrix $\boldsymbol{H}$ under different rotation angles of the transmitter. We can see that perfect link alignment (i.e., the transmitter rotation angle is 0°) yields the minimum condition number.

Generally, an excellent channel state is required for reliable signal transmission. We can set a threshold τ on the condition number κ and assume a good link quality for $\kappa \leq \tau$. For example, for $\tau = 4$, the maximum allowed rotation angle of transmitter is 12°, as seen from Fig. 10. Moreover, the condition number first increases gradually as the transmitter rotation angle increases, but then suddenly drops when rotation angle is 17°. That is because the channel quality deteriorates as the transmitter rotates. When the rotation angle exceeds a certain value, the PD cannot receive any optical signal, and all sub-channels have poor performance, resulting in small condition number.

Fig. 11 illustrates the change of the condition number as the receiver horizontally moves. It is seen that as the receiver moves away, the condition number increases gradually, showing the

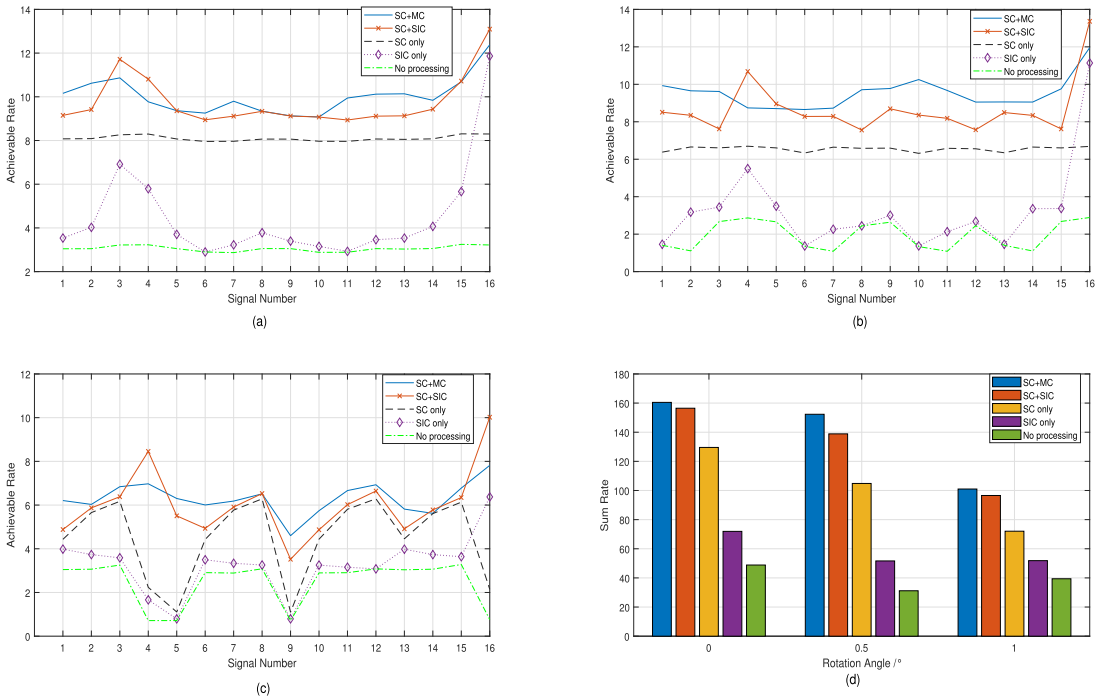

Fig. 13. Comparison of achievable rates using different signal processing methods. (a) Center aligned. (b) Receiver rotates $0.5°$. (c) Receiver rotates $1°$. (d) Sum rate under different rotation angles.

transmission performance is getting worse. Specifically, the receiver Δ_h can be up to 3.7 while maintaining a good transmission link with $\tau = 4$.

In vertical direction, the transmitter (or receiver) has a large allowed moving range because the light rays are nearly parallel. For $\tau = 4$, the transmitter can move about ± 1 m. Fig. 12 shows the light spots on detector plane for $\Delta_v = 370$. It is clear that each light spot can be distinguished and completely received by the PD. This demonstrates the robustness of the lens structure to vertical movement.

Notwithstanding, the receiver has a small allowed rotation angle less than 1° because rotation can seriously affect the effective reception area. Therefore, PD cannot receive any signal at all for rotation angle greater than 1°.

B. Signal Processing Results

In this subsection, we compare the results of multiple signal processing methods and discuss their performance.

First, we consider the parameters in multi-layer coding and group decoding. It has been proved that more layers and larger group numbers both lead to improved performance [24]. Considering complexity, we assume that users' messages are split into 3 parts, i.e., for $i = 1, 2, 3 \ldots 16$, all L_i equal to 3. For MC, the input signal obeys a TG distribution and $\mu_{ik} = 3\upsilon_{ik}$ at each layer. Using algorithm in [29], the optimal decoding order and the overall rate can be obtained.

We present the numerical results of achievable rate using signal combining with multi-layer coding (SC+MC), as well as the successive interference cancellation (SC+SIC) under different mobile situations. For comparison, we also calculate the achievable rate in the case of SC only, SIC only and no processing. Specifically, SC only refers to the approach where the signals are combined without cancelling interference and the weight vector is obtained by maximizing SINR; SIC only refers to the approach where the SIC is performed without signal combining; and no processing refers to merely treating interference as noise.

First we discuss the situation of receiver rotation. Figs. 13(a)–(c) show the achievable rate of each signal at different rotation angles. As we can see, whether in alignment or deviation, both SC+MC and SC+SIC provide significant sum rate improvement over the case of no processing. When the receiver rotates $0°$, the original rates of all signals are almost the same in Fig. 13(a), implying equal interference intensity among different signals. As interference cancellation proceeds, the last signal to be decoded will achieve the maximum transmission rate. However, SC+MC is not always better than MC+SIC for each signal in Figs. 13(a)–(c), due to different order of interference cancellation.

Fig. 13(d) shows the sum rates under different rotation angles. Apparently, the maximum sum rate is obtained when using SC+MC. As we described before, the MC scheme provides decoding system with more freedom and achieve better performance than SIC. The gap between SC+MC and SC+SIC can certainly prove this point.

For interference channel, SIC+SC yields more significant rate improvement than SIC only. The joint implementation of signal combining and interference cancellation can effectively utilize the information of strong signals, increasing the original sum rate by more than 3 times when the transmitter and receiver are aligned.

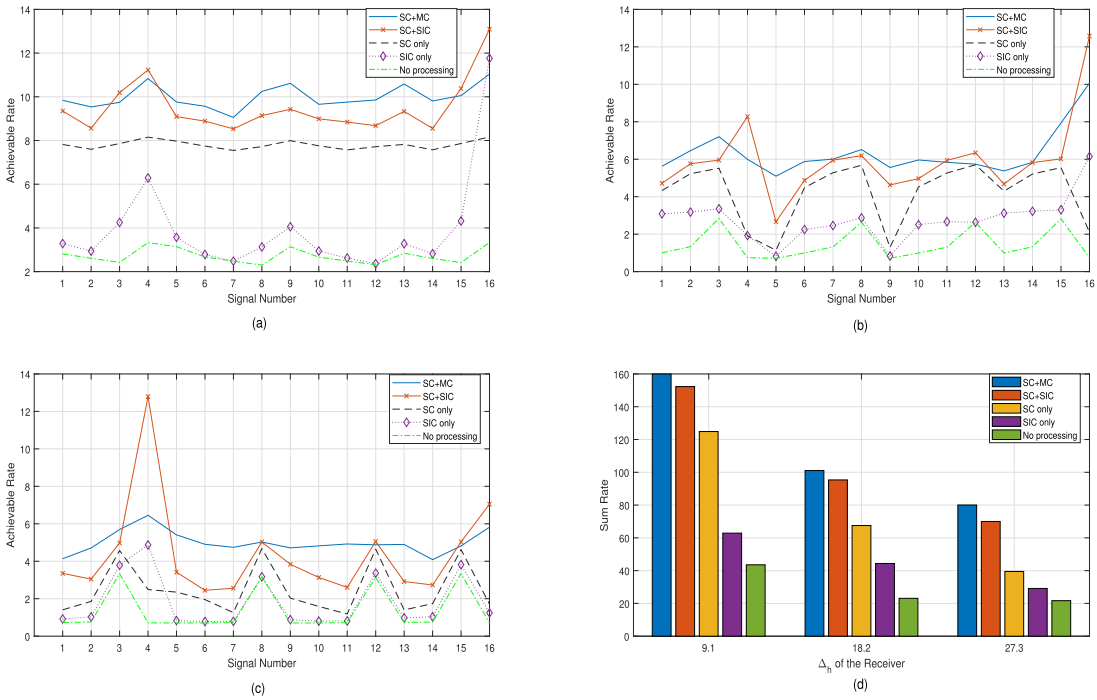

Fig. 14. Comparison of achievable rates using different signal processing methods. (a) Receiver $\Delta_h = 9.1$. (b) Receiver $\Delta_h = 18.2$. (c) Receiver $\Delta_h = 27.3$. (d) Sum rate at different Δ_h.

Next we investigate the case where the receiver horizontally moves, as shown in Fig. 14. The receiver has a limited moving distance in the horizontal direction because of small receiving area. But adding PDs and signal processing could effectively improve mobility. Expanding the PD array to 8×8, the maximum receiver Δ_h allowed increases from 3.7 to 27.3 for $\tau = 4$. Therefore, when the 8×8 PD array horizontally moves by 50 mm ($\Delta_h = 9.1$), the achievable rate with no processing is almost the same as that when the system is aligned as shown in Fig. 14(a).

Figs. 14(a)–(c) show the rate of each signal when the receiver horizontally moves. We can see the green polyline, corresponding to the original rate, gradually gets closer to 0 as the interference intensity increases. Although SC+MC and SC+SIC greatly improve system performance, the rates of most processed signals decrease as the receiver moves due to the decease of received power (see signal 5 for example).

In Fig. 14(d), as we expected, the highest sum rate is obtained by SC+MC. As the moving distance increases, the sum rate decreases for all processing approaches. We also see that both SC+SIC and SC+MC increase the sum rate by more than 3 times when $\Delta_h = 9.1$, compared with no processing. It is interesting to see that as the moving distance increases, the sum rate without processing first decreases and then increases, while the sum rate with SC+MC gradually decreases. This is because moving 100 mm ($\Delta_h = 18.2$) results in stronger interference than moving 150 mm ($\Delta_h = 27.3$), which is not necessarily harmful if interference decoding and cancellation are adopted.

The joint signal combining and interference cancellation can effectively utilize the desired signal and achieve better system performance. Whether the transmitter and receiver are aligned or not, the proposed approaches can significantly improve the achievable rate.

TABLE III
ACHIEVABLE RATE UNDER DIFFERENT LINKS

Channel	LOS link	LOS+NLOS link (VLC system at the center of the room)	LOS+NLOS link (VLC system in the corner of the room)
Sum Rate (bits/symbol)	160.49	157.42	153.12

We further consider the influence of NLOS links. In addition to the scenario where system is located at the room center, we consider the scenario where the receiver is located at the corner close to the wall. The LED array is placed 10 cm away from the wall, and the PD array is aligned with LED. We compare the achievable rates using SC+MC, as shown in Table III. The results show that the rate loss due to reflection is below 5%.

The proposed system has a meter-level dynamic range in the vertical direction. We fix the transmitter and receiver parameters (e.g., parameters of LEDs, PDs and lens) as those in the 5-m MIMO VLC system and vary the transmission distance. Fig. 15 shows the achievable sum rates by using SC+MC at transmission distances from 3 m to 8 m. We can see that 80% of the sum rate at 5-m distance can be achieved in the distance range of 4∼7 m, and the sum rate drops more quickly as the moving distance further increases. Moreover, the sum rate drops more slowly as the transmission distance increases compared with that

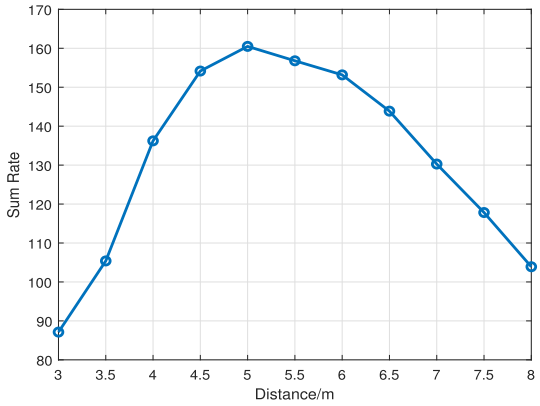

Fig. 15. Sum rate versus transmission distance.

as the transmission distance decreases. The results demonstrate the robustness of the proposed technique to the transmission distance in a certain range.

VI. Conclusion

In this paper, we have proposed a long-distance MIMO VLC system and the corresponding signal processing method considering the misalignment due to transmitter/receiver mobility. We have adopted one convex and one concave lenses as the optical antennas and optimize their structures to reduce the inter-LED interference. At 5-m communication distance, spots of 4×4 LEDs can be well separated on the receiving plane with obvious contour shape, which shows that each PD can receive the signal from corresponding LED with low interference. Moreover, we have investigated the transmission performance for the scenarios where the transmitter and the receiver are not perfectly aligned. We have adopted the signal combining and interference cancellation methods based on MC and SIC. Numerical results show that the achievable rate can be significantly improved via these methods.

References

[1] N. Chi, Y. Zhou, Y. Wei, and F. Hu, "Visible light communication in 6G: Advances, challenges, and prospects," *IEEE Veh. Technol. Mag.*, vol. 15, no. 4, pp. 93–102, Dec. 2020.

[2] Y. Wang, N. Chi, Y. Wang, L. Tao, and J. Shi, "Network architecture of a high-speed visible light communication local area network," *IEEE Photon. Technol. Lett.*, vol. 27, no. 2, pp. 197–200, Jan. 2015.

[3] M. Rahaim, I. Abdalla, M. Ayyash, H. Elgala, A. Khreishah, and T. D. Little, "Welcome to the CROWD: Design decisions for coexisting radio and optical wireless deployments," *IEEE Netw.*, vol. 33, no. 5, pp. 174–182, Sept./Oct. 2019.

[4] J. R. Barry, J. M. Kahn, W. J. Krause, E. A. Lee, and D. G. Messerschmitt, "Simulation of multipath impulse response for indoor wireless optical channels," *IEEE J. Sel. Areas Commun.*, vol. 11, no. 3, pp. 367–379, Apr. 1993.

[5] K. Lee, H. Park, and J. R. Barry, "Indoor channel characteristics for visible light communications," *IEEE Commun. Lett.*, vol. 15, no. 2, pp. 217–219, Feb. 2011.

[6] C. Chen, D. Basnayaka, and H. Haas, "Non-line-of-sight channel impulse response characterisation in visible light communications," in *Proc. IEEE Int. Conf. Commun.*, 2016, pp. 1–6.

[7] X. Nan, P. Wang, L. Guo, L. Huang, and Z. Liu, "A novel VLC channel model based on beam steering considering the impact of obstacle," *IEEE Commun. Lett.*, vol. 23, no. 6, pp. 1003–1007, Jun. 2019.

[8] P. Ge, X. Ling, J. Wang, X. Liang, S. Li, and C. Zhao, "Optical filter bank modeling and design for multi-color visible light communications," *IEEE Photon. J.*, vol. 13, no. 1, Feb. 2021, Art. no. 7901219.

[9] F. Miramirkhani and M. Uysal, "Channel modeling and characterization for visible light communications," *IEEE Photon. J.*, vol. 7, no. 6, Dec. 2015, Art. no. 905616.

[10] H. B. Eldeeb, M. Uysal, S. M. Mana, P. Hellwig, J. Hilt, and V. Jungnickel, "Channel modelling for light communications: Validation of ray tracing by measurements," in *Proc. 12th IEEE Int. Symp. Commun. Syst. Netw. Digit. Signal Process.*, 2020, pp. 1–6.

[11] H. B. Eldeeb, S. M. Mana, V. Jungnickel, P. Hellwig, J. Hilt, and M. Uysal, "Distributed MIMO for Li-Fi: Channel measurements, Ray tracing and throughput analysis," *IEEE Photon. Technol. Lett.*, vol. 33, no. 16, pp. 916–919, Aug. 2021.

[12] Q. Wang, Z. Wang, and L. Dai, "Multiuser MIMO-OFDM for visible light communications," *IEEE Photon. J.*, vol. 7, no. 6, Dec. 2015, Art. no. 7904911.

[13] K. Werfli *et al.*, "Experimental demonstration of high-speed $4\times$ 4 imaging multi-CAP MIMO visible light communications," *IEEE/OSA J. Lightw. Technol.*, vol. 36, no. 10, pp. 1944–1951, May 2018.

[14] M. Shi, C. Wang, G. Li, Y. Liu, K. Wang, and N. Chi, "A 5 Gb/s $2\times$ 2 MIMO real-time visible light communication system based on silicon substrate LEDs," in *Proc. Glob. LiFi Congr.*, 2019, pp. 1–5.

[15] C. Chen *et al.*, "User-centric MIMO techniques for indoor visible light communication systems," *IEEE Syst. J.*, vol. 14, no. 3, pp. 3202–3213, Sep. 2020.

[16] L. Zhao, K. Cai, and M. Jiang, "Multiuser precoded MIMO visible light communication systems enabling spatial dimming," *IEEE/OSA J. Lightw. Technol.*, vol. 38, no. 20, pp. 5624–5634, Oct. 2020.

[17] L. Zheng and D. N. C. Tse, "Diversity and multiplexing: A fundamental tradeoff in multiple-antenna channels," *IEEE Trans. Inf. Theory*, vol. 49, no. 5, pp. 1073–1096, May 2003.

[18] T. Q. Wang, Y. A. Sekercioglu, and J. Armstrong, "Analysis of an optical wireless receiver using a hemispherical lens with application in MIMO visible light communications," *IEEE/OSA J. Lightw. Technol.*, vol. 31, no. 11, pp. 1744–1754, Jun. 2013.

[19] T. Chen, L. Liu, B. Tu, Z. Zheng, and W. Hu, "High-spatial-diversity imaging receiver using fisheye lens for indoor MIMO VLCs," *IEEE Photon. Technol. Lett.*, vol. 26, no. 22, pp. 2260–2263, Nov. 2014.

[20] A. Iwasa, C. B. Naila, K. Kobayashi, H. Okada, and M. Katayama, "Experimental evaluation of an indoor long distance high speed imaging MIMO system," in *Proc. IEEE Glob. Commun. Conf.*, 2020, pp. 1–6.

[21] E. Xie *et al.*, "Over 10 Gbps VLC for long-distance applications using a GaN-based series-biased micro-LED array," *IEEE Photon. Technol. Lett.*, vol. 32, no. 9, pp. 499–502, May 2020.

[22] S. Yang and L. Hanzo, "Fifty years of MIMO detection: The road to large-scale MIMOs," *IEEE Commun. Surv. Tut.*, vol. 17, no. 4, pp. 1941–1988, Nov. 2015.

[23] T. Han and K. Kobayashi, "A new achievable rate region for the interference channel," *IEEE Trans. Inf. Theory*, vol. 27, no. 1, pp. 49–60, Jan. 1981.

[24] C. Gong, A. Tajer, and X. Wang, "Interference channel with constrained partial group decoding," *IEEE Trans. Commun.*, vol. 59, no. 11, pp. 3059–3071, Nov. 2011.

[25] S.-B. Li, C. Gong, P. Wang, and Z. Xu, "Lens design for indoor MIMO visible light communications," *Opt. Commun.*, vol. 389, pp. 224–229, Apr. 2017.

[26] E. Kurniawan and S. Sun, "Improper Gaussian signaling scheme for the Z-interference channel," *IEEE Trans. Wireless Commun.*, vol. 14, no. 7, pp. 3912–3923, Jul. 2015.

[27] J. Blomer and N. Jindal, "Transmission capacity of wireless ad hoc networks: Successive interference cancellation vs. joint detection," in *Proc. Int. Conf. Commun.*, 2009, pp. 1–5.

[28] G. Zheng, C. Gong, and Z. Xu, "Constrained partial group decoding with max-min fairness for multi-color multi-user visible light communication," *IEEE Trans. Commun.*, vol. 67, no. 12, pp. 8573–8584, Dec. 2019.

[29] C. Gong, A. Tajer, and X. Wang, "A practical coding scheme for interference channel using constrained partial group decoder," in *Proc. IEEE Glob. Telecommun. Conf.*, 2011, pp. 1–5.

[30] W. Liu, Z. Xu, and X. Jin, "Saturation compensation for visible light communication with off-the-shelf detectors," *Opt. Exp.*, vol. 29, no. 6, pp. 9670–9684, Mar. 2021.